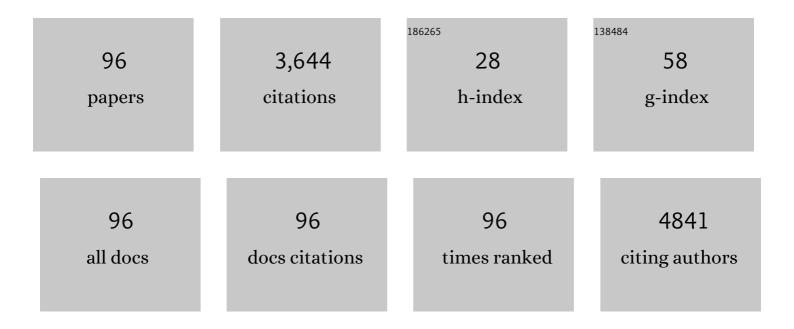
List of Publications by Year in descending order

Source: https://exaly.com/author-pdf/2848741/publications.pdf Version: 2024-02-01



I EI SUI

#	Article	IF	CITATIONS
1	Novel Iron/Cobaltâ€Containing Polypyrrole Hydrogelâ€Derived Trifunctional Electrocatalyst for Selfâ€Powered Overall Water Splitting. Advanced Functional Materials, 2017, 27, 1606497.	14.9	320
2	Engineering electrocatalytic activity in nanosized perovskite cobaltite through surface spin-state transition. Nature Communications, 2016, 7, 11510.	12.8	316
3	Ultra-long-life and highly reversible Zn metal anodes enabled by a desolvation and deanionization interface layer. Energy and Environmental Science, 2021, 14, 3120-3129.	30.8	250
4	Bimetallic nickel-molybdenum/tungsten nanoalloys for high-efficiency hydrogen oxidation catalysis in alkaline electrolytes. Nature Communications, 2020, 11, 4789.	12.8	192
5	Identification of Cu(100)/Cu(111) Interfaces as Superior Active Sites for CO Dimerization During CO ₂ Electroreduction. Journal of the American Chemical Society, 2022, 144, 259-269.	13.7	171
6	Nobleâ€Metalâ€Free Janusâ€like Structures by Cation Exchange for Zâ€Scheme Photocatalytic Water Splitting under Broadband Light Irradiation. Angewandte Chemie - International Edition, 2017, 56, 4206-4210.	13.8	166
7	Structure Sensitivity of Auâ€īiO ₂ Strong Metal–Support Interactions. Angewandte Chemie - International Edition, 2021, 60, 12074-12081.	13.8	161
8	Quadruple perovskite ruthenate as a highly efficient catalyst for acidic water oxidation. Nature Communications, 2019, 10, 3809.	12.8	150
9	Synthesis of Subâ€2 nm Ironâ€Doped NiSe ₂ Nanowires and Their Surfaceâ€Confined Oxidation for Oxygen Evolution Catalysis. Angewandte Chemie - International Edition, 2018, 57, 4020-4024.	13.8	133
10	Enhanced visible-light photocatalytic activity of Bi2MoO6 nanoplates with heterogeneous Bi2MoO6-x@Bi2MoO6 core-shell structure. Applied Catalysis B: Environmental, 2018, 224, 692-704.	20.2	116
11	The role of oxygen vacancies in water oxidation for perovskite cobalt oxide electrocatalysts: are more better?. Chemical Communications, 2019, 55, 1442-1445.	4.1	100
12	Size-dependent magnetic properties and Raman spectra of La2NiMnO6 nanoparticles. Journal of Applied Physics, 2009, 106, .	2.5	97
13	Amorphous Molybdenum Sulfide/Carbon Nanotubes Hybrid Nanospheres Prepared by Ultrasonic Spray Pyrolysis for Electrocatalytic Hydrogen Evolution. Small, 2017, 13, 1700111.	10.0	70
14	Evidence of short-range magnetic ordering above TC in the double perovskite La2NiMnO6. Applied Physics Letters, 2007, 91, 172505.	3.3	69
15	Near room-temperature magnetoresistance effect in double perovskite La2NiMnO6. Applied Physics Letters, 2013, 102, .	3.3	64
16	Single crystalline quaternary sulfide nanobelts for efficient solar-to-hydrogen conversion. Nature Communications, 2020, 11, 5194.	12.8	64
17	Ferromagnetism inLaCoO3nanoparticles. Physical Review B, 2007, 76, .	3.2	62
18	Nobleâ€Metalâ€Free Janusâ€like Structures by Cation Exchange for Zâ€Scheme Photocatalytic Water Splitting under Broadband Light Irradiation. Angewandte Chemie, 2017, 129, 4270-4274.	2.0	62

#	Article	IF	CITATIONS
19	Strongly Coupled Cobalt Diselenide Monolayers for Selective Electrocatalytic Oxygen Reduction to H ₂ O ₂ under Acidic Conditions. Angewandte Chemie - International Edition, 2021, 60, 26922-26931.	13.8	61
20	Griffiths phase, spin-phonon coupling, and exchange bias effect in double perovskite Pr2CoMnO6. Journal of Applied Physics, 2014, 116, .	2.5	58
21	Nature of short-range ferromagnetic ordered state above TC in double perovskite La2NiMnO6. Applied Physics Letters, 2010, 96, .	3.3	56
22	Size-dependent exchange bias in half-doped manganite nanoparticles. Applied Physics Letters, 2008, 93, .	3.3	52
23	Catalytic asymmetric C–Si bond activation via torsional strain-promoted Rh-catalyzed aryl-Narasaka acylation. Nature Communications, 2020, 11, 4449.	12.8	43
24	Theoretical study of size-dependent properties of BN nanotubes with intrinsic defects. Physical Review B, 2007, 76, .	3.2	42
25	Sr and Pb co-doping effect on the crystal structure, dielectric and magnetic properties of BiFeO3 multiferroic compounds. Journal of Alloys and Compounds, 2017, 708, 93-98.	5.5	40
26	Size-dependent structure and magnetic properties of DyMnO3 nanoparticles. Journal of Applied Physics, 2014, 116, .	2.5	34
27	Room-temperature multiferroicity in CeFeO3 ceramics. Journal of Alloys and Compounds, 2019, 797, 363-369.	5.5	34
28	Synthesis of Subâ€2â€nm Ironâ€Doped NiSe ₂ Nanowires and Their Surfaceâ€Confined Oxidation for Oxygen Evolution Catalysis. Angewandte Chemie, 2018, 130, 4084-4088.	2.0	33
29	Controllable Synthesis of Cu ₂ O Microcrystals via a Complexantâ€Assisted Synthetic Route. European Journal of Inorganic Chemistry, 2010, 2010, 1103-1109.	2.0	26
30	Nature of ferromagnetic ordered state in LaCoO3 epitaxial nano-thin film on LaAlO3 substrate. Journal of Alloys and Compounds, 2014, 594, 158-164.	5.5	23
31	The influence of substrate orientation and annealing condition on the properties of LaMnO3 thin films grown by polymer-assisted deposition. Applied Surface Science, 2015, 351, 188-192.	6.1	23
32	Synthesis, surface group modification of 3D MnV2O6 nanostructures and adsorption effect on Rhodamine B. Materials Research Bulletin, 2012, 47, 1725-1733.	5.2	22
33	Reduction-Controlled Atomic Migration for Single Atom Alloy Library. Nano Letters, 2022, 22, 4232-4239.	9.1	20
34	Local Valence and Hole-Doping Effect on Magnetic Properties in Double Perovskite La2NiMnO6. Journal of Superconductivity and Novel Magnetism, 2013, 26, 3287-3292.	1.8	19
35	Effects of Co and Mn doping on the structure and superconductivity of. Solid State Communications, 2008, 147, 27-30.	1.9	18
36	Simple polymer assisted deposition and strain-induced ferromagnetism of LaCoO3 epitaxial thin films. Surface and Coatings Technology, 2013, 226, 108-112.	4.8	18

#	Article	IF	CITATIONS
37	Spin-phonon coupling in R2CoMnO6 (R = Pr, Nd, Sm) thin films under biaxial compressive strain. Journal of Applied Physics, 2016, 120, .	2.5	18
38	Interaction of Iron Atoms with Pristine and Defective (8, 0) Boron Nitride Nanotubes. Journal of Physical Chemistry C, 2008, 112, 13571-13578.	3.1	17
39	Facile synthesis of Ca-doped manganite nanoparticles by a nonaqueous sol–gel method and their magnetic properties. Materials Chemistry and Physics, 2010, 120, 75-78.	4.0	17
40	Radiation-Induced Inclusion Polymerization of Acrylonitrile in Urea Canals: Toward Synthesis of Completely Isotactic Polyacrylonitrile with Controlled Molecular Weight. Macromolecules, 2013, 46, 1765-1771.	4.8	17
41	Short-Range Magnetic Ordered State Above T C in Double Perovskite Dy 2 NiMnO 6. Journal of Superconductivity and Novel Magnetism, 2015, 28, 53-59.	1.8	17
42	Direct Growth of CoFe ₂ Alloy Strongly Coupling and Oxygenâ€Vacancyâ€Rich CoFe ₂ O ₄ Porous Hollow Nanofibers: an Efficient Electrocatalyst for Oxygen Evolution Reaction. Energy Technology, 2018, 6, 2350-2357.	3.8	17
43	Pt-Anchored CuCrO ₂ for Low-Temperature-Operating High-Performance H ₂ S Chemiresistors. ACS Applied Materials & Interfaces, 2022, 14, 24536-24545.	8.0	17
44	Direct Observation of Magneticâ€lon Offâ€Centeringâ€lnduced Ferroelectricity in Multiferroic Manganite Pr(Sr _{0.1} Ca _{0.9}) ₂ Mn ₂ O ₇ . Advanced Materials, 2015, 27, 6328-6332.	21.0	14
45	Tuning of magnetic properties for epitaxial Y2NiMnO6 thin film: Substrate is crucial. Applied Surface Science, 2016, 384, 459-465.	6.1	14
46	Strain effect on the transport properties of epitaxial PrNiO ₃ thin films grown by polymer-assisted deposition. Journal Physics D: Applied Physics, 2016, 49, 125301.	2.8	13
47	Superconductivity and the disorder effect in Ag and Al double doped MgB2. Journal of Applied Physics, 2006, 100, 023905.	2.5	12
48	High-temperature thermoelectric characteristics of B-site substituted Yb0.1Ca0.9Mn1â^'x Nb x O3 system (0â‰ ¤ â‰ 9 .1). Applied Physics A: Materials Science and Processing, 2013, 112, 1003-1009.	2.3	12
49	Spin-Reorientation Transition Driven by Double Exchange in CeFeO ₃ Ceramics. Journal of Physical Chemistry C, 2020, 124, 15399-15405.	3.1	12
50	Tuning the metal-insulator transition via epitaxial strain and Co doping in NdNiO3 thin films grown by polymer-assisted deposition. Journal of Applied Physics, 2016, 119, .	2.5	11
51	Tunability of magnetization and bandgap in mullite-type Bi2Fe4O9 ceramics through non-magnetic ions. Scripta Materialia, 2018, 146, 55-59.	5.2	11
52	Anomalous magnetism in Al doped La2CoMnO6 ceramics. Journal of Magnetism and Magnetic Materials, 2020, 510, 166950.	2.3	11
53	Structure Sensitivity of Auâ€īiO 2 Strong Metal–Support Interactions. Angewandte Chemie, 2021, 133, 12181-12188.	2.0	11
54	Insight into the Magnetization Reversal and Exchange Bias in RFe _{0.5} Cr _{0.5} O ₃ Ceramics. Journal of Physical Chemistry C, 2021, 125, 7950-7958.	3.1	11

#	Article	IF	CITATIONS
55	Theoretical Study of the Site-Dependent Stabilities of Intrinsic Defects in a Polar BN Nanotube with Finite Length. Journal of Physical Chemistry C, 2008, 112, 19353-19359.	3.1	10
56	Fabrication of Polyaniline/Silver Nanocomposite Under Gamma-ray Irradiation. Chinese Journal of Chemical Physics, 2010, 23, 701-706.	1.3	10
57	Size-induced transition from non–Griffiths-like to Griffiths-like clustered phase above the Curie temperature. Europhysics Letters, 2012, 98, 57004.	2.0	10
58	Spin-State Transition Enhanced Oxygen Evolving Activity in Misfit-Layered Cobalt Oxide Nanosheets. ACS Sustainable Chemistry and Engineering, 2018, 6, 12337-12342.	6.7	10
59	Tunability of Bandgap and Magnetism in K and Pb Codoped BiFeO ₃ Nanoparticles for Multiferroic Applications: The Role of Structural Transition and Fe Deficiency. ACS Applied Nano Materials, 2019, 2, 1995-2004.	5.0	10
60	Tuning Ferroelectric, Dielectric, and Magnetic Properties of BiFeO ₃ Ceramics by Ca and Pb Coâ€Doping. Physica Status Solidi (B): Basic Research, 2019, 256, 1800499.	1.5	10
61	Susceptibility behaviour and specific heat anomaly in single crystals of alanine and valine. Journal of Biological Physics, 1996, 22, 65-71.	1.5	9
62	Optical Study of Nanosize Effects on Charge Ordering in Half-Doped Manganites. Journal of Physical Chemistry C, 2013, 117, 8989-8996.	3.1	9
63	Spin-polarized electron transport in highly reduced MgFe ₂ O _{4-<i>δ</i>} . Materials Research Express, 2018, 5, 126301.	1.6	9
64	A-site ion-size effect on the transport and magnetic properties of Ce doping Pr0.3Ce0.2CaxSr0.5â^'xMnO3 (0â‰ ¤ â‰ 0 .25). Journal of Applied Physics, 2011, 109, .	2.5	8
65	Structural characteristics, magnetic properties of Re2NiMnO6 (Re=La, Pr, Nd, Sm, Y) thin films on (001) LaAlO3 by simple polymer assisted deposition. Surface and Coatings Technology, 2015, 277, 222-226.	4.8	8
66	Insight into the enhancement of transport property for oriented La _{0.9} MnO ₃ films. Journal Physics D: Applied Physics, 2017, 50, 205306.	2.8	8
67	Bio-inspired synthesis of transition-metal oxide hybrid ultrathin nanosheets for enhancing the cycling stability in lithium-ion batteries. Nano Research, 2022, 15, 5064-5071.	10.4	8
68	Electrorheological properties and structure of (BaTiO(C2O4)2/NH2CONH2). Journal of Solid State Chemistry, 2006, 179, 1874-1878.	2.9	7
69	Characterization upon electrical hysteresis and thermal diffusion of TiAl3O x dielectric film. Nanoscale Research Letters, 2011, 6, 557.	5.7	7
70	Nature of Griffiths phase and ferromagnetic 3d-4f interaction in double-perovskite Dy2CoMnO6. Journal of Alloys and Compounds, 2022, 893, 162222.	5.5	7
71	Tuning the magnetic and transport properties of La0.8Ca0.2MnO3 films by Ba0.8Sr0.2TiO3 intercalated layers grown with polymer-assisted deposition. Applied Physics Letters, 2017, 110, 231602.	3.3	6
72	High-temperature metal–insulator transition in YxCa1â^'xMnO3 (0.05⩽x⩽0.12): An electron-spin reso study. Journal of Alloys and Compounds, 2014, 582, 37-42.	nance 5.5	5

#	Article	IF	CITATIONS
73	The effect of charge transfer on the transport and magnetic properties induced by Ca substitution in La0.3Ce0.2Sr0.5MnO3. Journal of Alloys and Compounds, 2017, 725, 349-354.	5.5	5
74	Orientation-adjusted anomalous insulator-metal transition in NdNiO3/LaMnO3 bilayers. Applied Physics Letters, 2018, 112, .	3.3	5
75	The effect of composite configurations of Fe ionic spins on the dielectric properties in Sm-doped CeFeO3 ceramics. Ceramics International, 2021, 47, 5767-5775.	4.8	5
76	Electronic property and structure of double-doping Y1â^'2xPrxCaxBa2Cu3O7â~'δ with 0⩽x⩽0.14. Physica Superconductivity and Its Applications, 2010, 470, 607-610.	C: 1.2	4
77	Interfacial coupling, oxygen deficiency, and orbital reconstruction in oriented La0.7Ca0.3MnO3/DyMnO3 bilayers. Applied Physics A: Materials Science and Processing, 2019, 125, 1.	2.3	4
78	Regioselective Construction of Chemically Transformed Phosphide–Metal Nanoheterostructures for Enhanced Hydrogen Evolution Catalysis. Inorganic Chemistry, 2021, 60, 7269-7275.	4.0	4
79	Electrical transport properties driven by magnetic competition in hole-doped perovskite Pr1-xBaxMnO3 (0.25 ≤ ≤0.36). Ceramics International, 2021, 47, 19464-19470.	4.8	4
80	Particle size effects on stripe ordering and magnetic properties in nanosized La5/3Sr1/3NiO4. Solid State Communications, 2008, 147, 258-261.	1.9	3
81	High magnetoresistance in layered PrBaCo2O5+δ double perovskite. Journal of Alloys and Compounds, 2020, 819, 153001.	5.5	3
82	Strain induced Co/Mn ionization and magnetic properties in double-perovskite Nd2CoMnO6 thin films. Journal of Applied Physics, 2020, 128, 145305.	2.5	3
83	Strongly Coupled Cobalt Diselenide Monolayers Selectively Catalyze Oxygen Reduction to H2O2 in an Acidic Environment. Angewandte Chemie, 0, , .	2.0	3
84	Effects on transition temperature and Raman spectra of substitution of Cr and Al for Mg in MgB2. Physica Status Solidi (B): Basic Research, 2007, 244, 3244-3253.	1.5	2
85	Change from electronlike to holelike carriers in MgCNi3 via doping with B or Zn. Materials Chemistry and Physics, 2013, 138, 743-746.	4.0	2
86	Resonance Effect of Ionic Valences on the Structural and Magnetic Properties of Dy 2 NiMnO 6 Induced by Nonmagnetic Al Ion Doping. Physica Status Solidi (B): Basic Research, 2019, 256, 1900168.	1.5	2
87	Strain-controlled oxygen content and the cationic electronegativity in LaBaCo2O5.5+δthin films. Journal of Applied Physics, 2021, 129, 175301.	2.5	2
88	Frontispiece: Strongly Coupled Cobalt Diselenide Monolayers for Selective Electrocatalytic Oxygen Reduction to H ₂ O ₂ under Acidic Conditions. Angewandte Chemie - International Edition, 2021, 60, .	13.8	2
89	Formation and Characteristics of Acrylonitrile/Urea Inclusion Compound. Chinese Journal of Chemical Physics, 2013, 26, 198-202.	1.3	1
90	Electronic Property of the C-Site Doped MgCNi. Journal of Superconductivity and Novel Magnetism, 2014, 27, 209-213.	1.8	1

#	Article	IF	CITATIONS
91	Study of the Effects of Aâ€Site Laâ€Substition on the Electrical and Magnetic Properties of Dy _{0.5} Sr _{0.5} MnO ₃ Ceramics. Physica Status Solidi (B): Basic Research, 2018, 255, 1700155.	1.5	1
92	Synthesis and Electrorheological Properties of LTNO-PS Composites. Chinese Journal of Chemical Physics, 2007, 20, 319-323.	1.3	0
93	Ferromagnetism Enhanced by Lattice Distortion in Fine La5/3Sr1/3NiO4 Particles. Journal of Superconductivity and Novel Magnetism, 2010, 23, 411-415.	1.8	0
94	Negative slope of resistivity–temperature curve and positive magnetoresistance in antiperovskite ZnCNi3â^'x Mn x (1.15≤â‰⊉.5). Applied Physics A: Materials Science and Processing, 2014, 114, 833-838.	2.3	0
95	SrFe1â^xMoxO2+δ : parasitic ferromagnetism in an infinite-layer iron oxide with defect structures induced by interlayer oxygen. Materials Research Express, 2018, 5, 046106.	1.6	0
96	Frontispiz: Strongly Coupled Cobalt Diselenide Monolayers for Selective Electrocatalytic Oxygen Reduction to H ₂ O ₂ under Acidic Conditions. Angewandte Chemie, 2021, 133, .	2.0	0